PHYSICAL REVIEW E **74**, 040701(R) (2006)

Stick-slip dynamics around a topological defect in free-standing smectic films

Alexey Eremin, Christian Bohley, and Ralf Stannarius
Otto-von-Guericke-University, Institute of Experimental Physics, Universitätsplatz 2, D-39106 Magdeburg, Germany
(Received 20 January 2006; published 9 October 2006)

We study the orientational relaxation of a spiral pattern around a central defect with topological strength $S=+1$ in free-standing smectic films. Instead of a continuous unwinding, a characteristic stick-slip relaxation is observed, where the elastic anisotropy plays the dominant role for the director anchoring in the vicinity of the defect. A model derived from nematic continuum theory is used to interpret the experimental observations.

DOI: 10.1103/PhysRevE.74.040701 PACS number(s): 61.30.Eb, 61.30.Jf, 05.90.+m

The dynamics of free-standing smectic films has attracted much scientific interest in recent decades for mainly two reasons. First, planar free-standing smectic C or C^* films with in-plane flow represent one of the simplest examples of anisotropic fluid dynamics, in quasi-two-dimensions. Second, in films of circular geometry, it is easy to prepare highly regular director and flow patterns using external mechanical or electrical fields. There has been a large number of studies describing flow or orientational relaxation phenomena in such films, e.g., [1–12]. In particular, the formation and relaxation of target and spiral patterns have been addressed experimentally and theoretically. The c director, marking the azimuth of the mesogenic tilt in the film plane, describes the local orientation state. The relaxation of c-director patterns can be monitored by polarizing microscopy. In this work, we focus on the relaxation dynamics around a central topological defect with strength $S=+1$. Mathematical treatment of such structures is particularly simple, owing to the cylindrical symmetry of the c-director field. The observation of the film at normal incidence with slightly decrossed polarizers in reflection yields textures of two-armed spirals (Fig. 1), from which the director field can be reconstructed. It has been confirmed experimentally that shear flow coupling to the c director can be neglected. This is not the case in the geometries of a defect-free target pattern or a central -1 defect [13]. An interesting aspect of the $+1$ configuration is the competition of bulk relaxation dynamics and anchoring of the c director at the defect. The elastic anisotropy of the material becomes essential in the vicinity of the center. It determines the character of the global relaxation, causing a regular oscillation between two types of solutions.

The first one is equivalent to the dynamics of the defect-free state described by a linear diffusion equation for the c-director angle, and exponential relaxation toward the homogeneous state [3]. In contrast, when the center of the film is occupied by some macroscopic particle that fixes the c director, this complete relaxation is inhibited and a stationary inhomogeneous director pattern is reached; its equilibrium state is also given by a differential equation (the Laplace equation in the one-elastic-constant approximation). In the case considered here, the relaxation dynamics near the central $+1$ defect oscillates between these two limits. Such highly nonlinear periodic dynamics is known as stick-slip motion (e.g., [14–18]). It is found in a widespread variety of physical systems and everyday life's observations, like the excitation of a violin string by a bow, vibrations of a ringing wine glass [15], earthquakes [16], molecular dynamics [17], or jamming of granular matter [18]. Here, the rotational viscosity of the material provides the friction term; energy differences for splay and bend deformations of the c director form a potential that hinders c-director relaxation.

We present experimental data and interpret them within a dynamic model. In addition to the description of the stick-slip phenomenon, the model provides quantitative access to the elastic anisotropy of the material.

Experiments have been performed with different smectic materials, where the observations are qualitatively identical. Exemplarily, we present results for the material shown in Fig. 2, with the phase sequence

$$\text{Crystalline} \xrightarrow{65\ ^\circ\text{C}} (\text{Sm}C_2) \xleftrightarrow{59\ ^\circ\text{C}} \text{Sm}C_1 \xleftrightarrow{66.5\ ^\circ\text{C}} \text{isotropic}.$$

The material is nonchiral; the not fully classified phases are a synclinic ($\text{Sm}C_1$) and a monotropic anticlinic ($\text{Sm}C_2$) tilted smectic phase, respectively [20]. Experiments are performed in the synclinic phase at 65 °C. Temperature is stabilized with a Linkam hot stage. The films are observed in an NU2 polarizing microscope (Carl Zeiss) equipped with a charge-coupled device camera. Images are taken at a constant rate and processed digitally.

Films are drawn across a circular hole (∅ 0.48 mm) in a support frame. The c director favors tangential anchoring at the meniscus; thus the c-director field necessarily has a total defect strength of $+1$. Four electrodes placed on the sample

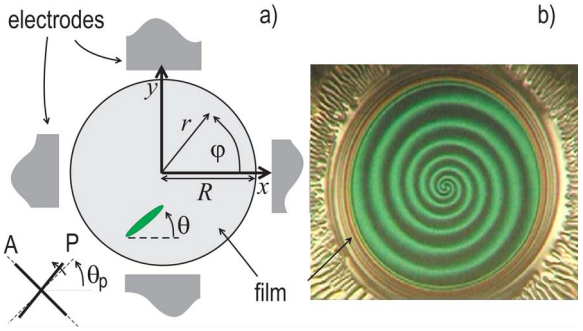

FIG. 1. (Color online) (a) Geometry of the experiment and definition of the variables. (b) Reflection image under slightly decrossed polarizers (P,A). The film appears bright where the c director is along y, and dark when the c director is along x (see text). The image is not stationary; the c director relaxes on a time scale of minutes. Image width 0.32 mm.

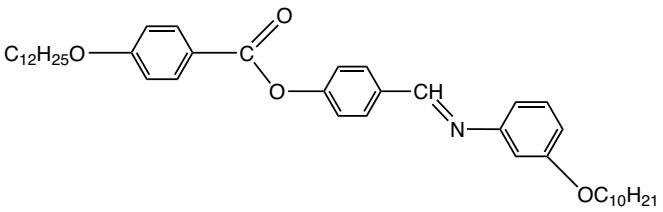

FIG. 2. Chemical composition of the investigated substance.

holder around the film allow one to apply rotating electric fields. The electric torque winds up the c director (as described, e.g., in [1]). Optimum rotation frequencies are a few hertz and field strengths around 10 kV/m. Since we are only interested in elastic relaxation, we disregard the behavior in the electric field and concentrate entirely on the dynamics after the field is switched off. In most experiments, one obtains a defect-free film center, with a +1 defect located at the outer border. Then one can approximate the film, disregarding the defect, by a pattern consisting of concentric rings of constant c-director orientation that relaxes continuously toward a uniformly oriented state [3]. In very few cases, spirals are formed with an $S=-1$ defect in the film center (and additional defects near the film boundary). Quite often, however, one obtains spirals with a single central $S=+1$ defect. After the electric field is switched off, the c director quickly adopts a cylindrically symmetric configuration; its texture is shown in Fig. 1. Dark brushes of the two-armed spiral mark regions where the c director is along $\pm x$ (horizontal in the image); bright areas correspond to regions with the c director along $\pm y$ (vertical in the image). The intensity variation with the c-director angle θ respective to the polarizer angle θ_p is approximately $\Delta I \propto \sin^2(\theta - \pi/4 - \theta_p)$. This optical characteristic is typical for low-birefringence samples in depolarized reflected light microscopy [19] images.

It is no coincidence that in the images of Figs. 1 and 3 the spiral ends in a tangential c-director configuration in the center [22]. There is some analogy with the situation where a small cylindrical particle of radius r_i with strong surface anchoring is trapped in the spiral center. We will discuss this simpler situation first, in the one-elastic-constant approximation. The tangential anchoring at the outer boundaries is taken as the reference, $\theta(R,\varphi)=\theta_R=\pi/2+\varphi$. In the center, the phase is $\theta(r_i,\varphi)=\pi/2+\varphi+\Delta\theta$, with a phase lag $\Delta\theta$ between center and meniscus. Since $\Delta\theta$ is fixed, the spiral reaches a stationary state before the c director is relaxed to the all-tangential configuration $\theta(r,\varphi)=\theta_R$. When the center of the spiral is not a particle but an $S=+1$ point defect, the situation is more complex. Even though the c director is not rigidly pinned at a surface, the spiral does not rotate continuously around the center (Figs. 3 and 4), since bend is energetically favored. Even small differences of the elastic constants K_b for bend and K_s for splay distortions lead to large energy differences near the defect, and stick-slip dynamics sets in. Two slip events are shown exemplarily in the two columns of Fig. 3. Note the concentration of the radial deformation near the central defect at constant total phase lag $\Delta\theta$ (the spiral arms contract in the center) immediately before the slips take place.

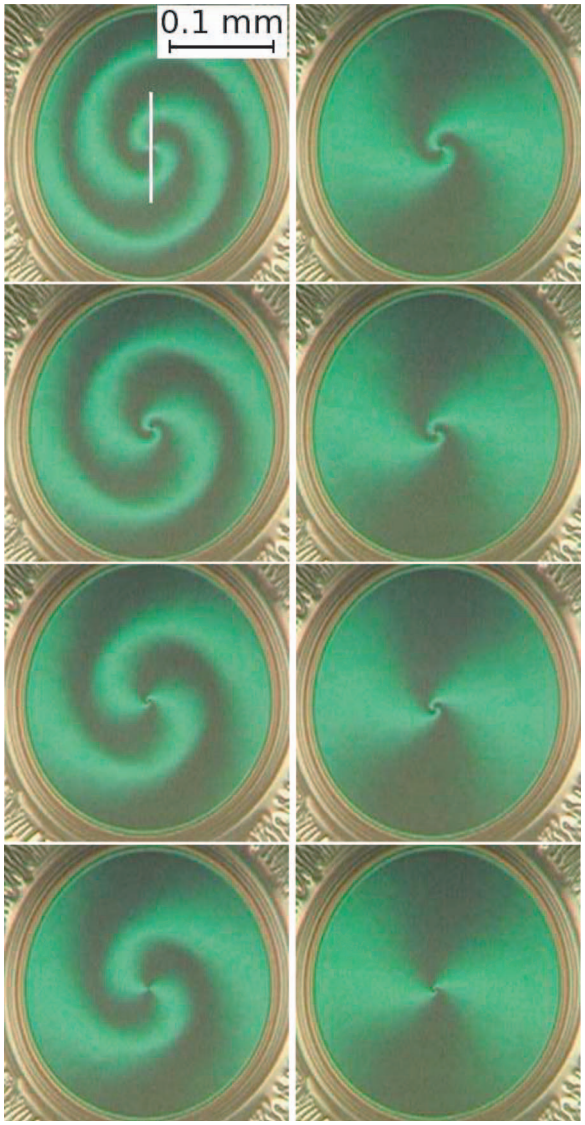

FIG. 3. (Color online) Spiral with a central $S=+1$ defect observed in reflection between slightly decrossed polarizers (diagonal in the images). The images in each column are recorded in steps of 4 s in an almost unwound spiral. In the left column, the slip from the $\Delta\theta=2\pi$ to the $\Delta\theta=\pi$ spiral is seen. The right column starts 12 s later, immediately before the last slip (π to 0) takes place. The vertical white line marks the cross section from which Fig. 4(a) below has been composed. The film thickness is approximately 30 layers.

Figure 4(a) shows a detail of the space-time plot. The spatial axis corresponds to the cross section marked by the white line in Fig. 3; it covers approximately one-half of the spiral diameter. From the optical textures, the known characteristics $\Delta I(\theta)$ and the assumption $\theta(r,\varphi)=\theta(r,0)+\varphi$, the radial profile of the phase has been determined [Fig. 4(b)]. The first three jumps are the same as in Fig. 4(a). While the outer spiral parts show a continuous, nearly uniform relaxation, there is an alternating sequence of nearly stationary states and discontinuous jumps near the center; this is particularly evident in Fig. 4(b). In the vicinity of the central defect, the c director in the spiral arms keeps its tangential orientation,

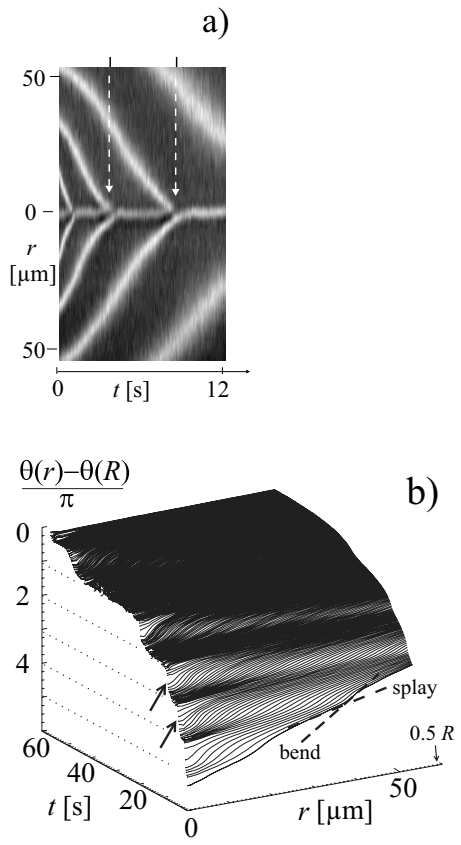

FIG. 4. (a) Space-time plot of the cross section of the optical images, taken along the white line in Fig. 3. Arrows point at two consecutive slips in the series. Between the slips, the c director near the defect remains fixed. (b) Radial director profile $\theta(r,0)$ evaluated from the optical textures; same experiment as in (a); arrows point to the same jumps. The different slopes in regions of bend and splay of the c-director field (dashed lines) indicate that K_s is roughly $4.5K_b$.

while the c-director field relaxes in the outer parts. Then, in a quick jump, the central part reorients by an angle π, releases elastic stress in the center, and adopts a tangential orientation again. In the following period, the spiral readjusts to the new phase difference and the deformation again concentrates in the central part, until another jump is performed. The plateaus formed near $r=0$ in Fig. 4(b) reflect the elastic anisotropy.

The analysis of a simplified dynamic model that assumes elastic isotropy, $K_b=K_s=K$, may qualitatively elucidate the nature of the jumps. The experimental observations show that flow in the film is absent. The torque balance equation for director relaxation in nematics can be directly adapted. Under the usual neglect of inertia, one arrives at the linear partial differential equation [3]

$$\frac{\partial^2\theta}{\partial r^2}+\frac{1}{r}\frac{\partial\theta}{\partial r}+\frac{1}{r^2}\frac{\partial^2\theta}{\partial\varphi^2}=\frac{1}{D}\frac{\partial\theta}{\partial t}, \tag{1}$$

with $D=K/\gamma$ and the rotational viscosity γ. The solutions of Eq. (1) that satisfy the boundary condition $\theta(R,\varphi,t)=\varphi+\pi/2$ are given by the expansion

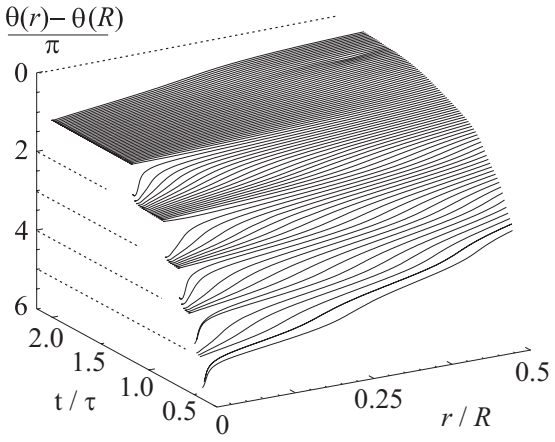

FIG. 5. Director angle $\theta(r,0)$ as a function of time, calculated numerically with the assumption $K_s=4.5K_b$. The time axis is scaled with $\tau=\gamma R^2/K$, and $t=0$ is chosen arbitrarily.

$$\theta(r,\varphi,t)=\theta_s(r,\varphi)+\sum_{k=1}^{\infty}\theta_k\exp(-Da_k^2t/R^2)J_0(a_kr/R) \tag{2}$$

where θ_s is a stationary solution, and a_k are the zeros of the Bessel function J_0. The sum reproduces the target pattern solution [3]. For a spiral around a fictive central particle with radius r_i and strong tangential anchoring,

$$\theta_s(r,\varphi)=n\pi\frac{\ln(r/R)}{\ln(r_i/R)}+\theta_R, \tag{3}$$

satisfies the boundary conditions at r_i and R. Such a spiral with initial phase lag $\Delta\theta=n\pi$ relaxes toward θ_s, since all terms of the sum decay toward zero with progressing time. When the anchoring is strong enough, the torque connected with the radial derivative $(d\theta_s/dr)|_{r_i}$ is compensated, and the relaxation terminates on approaching θ_s. The film thickness d plays no role, since all energies and forces scale linearly with d.

It is evident that the torque exerted by the c director at r_i increases when the higher terms in the expansion in Eq. (2) decay and $\theta(r,\varphi)$ converges toward Eq. (3). In case of weak anchoring and sufficiently high initial distortion $n\pi$, the fixed orientation at r_i is finally given up and the director flips by 180°. The relaxation of the new c-director field then continues toward a logarithmic spiral with the new phase lag $(n-1)\pi$. This process provides the explanation of the dynamics around an $S=+1$ defect. In the absence of a central particle, even a small elastic anisotropy becomes essential near the defect, where the elastic distortion energy diverges. It creates some energy barrier that can be regarded as an effective anchoring potential.

The elastic free-energy density f in the immediate vicinity of the defect, where $\alpha=\theta-\varphi$ is approximately constant, can be written as $f=\frac{1}{2}(K+\delta K\cos 2\alpha)r^{-2}$ where $\delta K=\frac{1}{2}(K_s-K_b)$, $K=\frac{1}{2}(K_s+K_b)$. The integral over a circular area around the defect gives

$$F(r_i) = \int_0^{2\pi} \int_\rho^{r_i} fr\, dr\, d\varphi = \pi(K + \delta K \cos 2\alpha) \ln\left(\frac{r_i}{\rho}\right)$$

where ρ is some core radius of the defect, estimated to be well below 1 μm, and r_i is a hypothetical radius within which α can be regarded as constant [plateaus near $r=0$ in Fig. 4(b)]. The α dependence of $F(r_i)$ is responsible for an effective tangential anchoring at r_i, it can sustain a torque density of the c director. The torque density actually exerted in the spiral is given by the radial derivative of θ. When the deformation converges toward the solution θ_s, the torque reaches sufficiently high values to overcome the anchoring potential.

Another qualitative feature for materials with $K_b \neq K_s$ is a modulation of the spiral arms in the alternating bend and splay regions [dashed lines in Fig. 4(b)]. The value for K_s/K_b given in the caption of Fig. 4 has been estimated from the local variation of the slope $d\theta_s/dr$ far from the center; details are given elsewhere [13].

While this discussion is useful for the qualitative explanation of the nature of the observed stick-slip process, a quantitative comparison of experiment and theory requires the analysis of the rigorous nonlinear equations with elastic anisotropy. We introduce the variable $u(r)=\theta(r,\varphi)-\theta(R,\varphi)$ so that the c director is given by $\mathbf{c}=(-\sin(u+\varphi),\cos(u+\varphi))$. The torque balance equation is derived from the standard free energy density [21] $f=\frac{1}{2}[K_s(\nabla\cdot\mathbf{c})^2+K_b(\nabla\times\mathbf{c})^2]$, by

$$\gamma\frac{\partial u}{\partial t} = \frac{\partial f}{\partial u} - \frac{d}{dx}\frac{\partial f}{\partial u_x} - \frac{d}{dy}\frac{\partial f}{\partial u_y}, \quad u_x = \frac{\partial u}{\partial x}, \quad u_y = \frac{\partial u}{\partial y}. \quad (4)$$

We seek a numerical solution of Eq. (4), using a finite-element algorithm (FEMLAB software). The computation starts with a quadratic profile with maximum deformation $\Delta\theta=\Delta u=10\pi$. After an initial period of the order of 0.35τ, the deformation amplitude has relaxed to $\approx 6\pi$, and the profile no longer depends upon details of the initial deformation. The further evolution of the calculated phase profile is shown in Fig. 5.

Although the computed data differ in details from the experiment, the undulations, and in particular the jumps, are reproduced satisfactorily well. Reasons for slight quantitative differences in details lie both in certain numerical difficulties related to the treatment of the equations in the vicinity of the central defect, and to a minor extent in the neglection of flow effects. We note that the mean exponential relaxation of $\Delta\theta$ is only marginally slower than the relaxation of the $k=0$ term in Eq. (2), i.e., the stick-slip mechanism has little effect on the overall relaxation dynamics.

The authors acknowledge the DFG for financial support within Project No. STA 425/20, W. Weissflog for supply of material, and J. Li, N. Mühlenrad, and I. Jähnert for participating in experiments.

[1] G. Hauck, H. D. Koswig, and C. Selbmann, Liq. Cryst. **21**, 847 (1996); C. Dascalu, G. Hauck, H. D. Koswig, and U. Labes, *ibid.* **21**, 733 (1996).
[2] C. Chevallard, T. Frisch, and J. M. Gilli, J. Phys. II **7**, 1261 (1997); C. Chevallard, J.-M. Gilli, T. Frisch, I. V. Chikina, and P. Pieranski, Mol. Cryst. Liq. Cryst. Sci. Technol., Sect. A **328**, 595 (1999).
[3] D. R. Link, L. Radzihovsky, G. Natale, J. E. Maclennan, N. A. Clark, M. Walsh, S. S. Keast, and M. E. Neubert, Phys. Rev. Lett. **84**, 5772 (2000).
[4] P. E. Cladis, Y. Couder, and H. R. Brand, Phys. Rev. Lett. **55**, 2945 (1985).
[5] P. E. Cladis and H. R. Brand, Liq. Cryst. **14**, 1327 (1993).
[6] P. E. Cladis, P. L. Finn, and H. R. Brand, Phys. Rev. Lett. **75**, 1518 (1995).
[7] P. Cladis and W. van Saarloos, in *Solitons in Liquids Crystals*, edited by L. Lam and J. Prost (Springer-Verlag, New York, 1992).
[8] A. Kilian, H.-D. Koswig, and A. Sonnet, Mol. Cryst. Liq. Cryst. Sci. Technol., Sect. A **265**, 321 (1995).
[9] I. Mutabazi, P. L. Finn, J. T. Gleeson, J. W. Goodby, C. D. Andereck, and P. E. Cladis, Europhys. Lett. **19**, 391 (1992).
[10] A. Becker, H. Stegemeyer, R. Stannarius, and St. Ried, Europhys. Lett. **39**, 257 (1997).
[11] S. W. Morris, J. R. de Bruyn, and A. D. May, Phys. Rev. Lett. **65**, 2378 (1990).
[12] H. Pleiner, R. Stannarius, and W. Zimmermann, in *Evolution of Spontaneous Structures in Dissipative Continuous Systems*, edited by H. Busse and S. C. Müller (Springer-Verlag, Heidelberg, 1998).
[13] A. Eremin, C. Bohley, and R. Stannarius, Phys. Rev. Lett. **97**, 097802 (2006).
[14] A. L. Demirel and S. Granick, Phys. Rev. Lett. **77**, 4330 (1996); M. Urbakh, J. Klafter, D. Gourdon, and J. Israelachwili, Nature (London) **430**, 525 (2004).
[15] Y.-Y. Chen, Am. J. Phys. **73**, 1045 (2005).
[16] J. M. Carlson and J. S. Langer, Phys. Rev. A **40**, 6470 (1989).
[17] U. Bockelmann, B. Essevaz-Roulet, and F. Heslot, Phys. Rev. Lett. **79**, 4489 (1997).
[18] I. Albert *et al.*, Phys. Rev. Lett. **84**, 5122 (2000).
[19] R. Pindak, C. Y. Young, R. B. Meyer, and N. A. Clark, Phys. Rev. Lett. **45**, 1193 (1980); C. D. Muzny and N. A. Clark, *ibid.* **68**, 804 (1992).
[20] B. Das, S. Grande, A. Eremin, M. Schröder, S. Diele, G. Pelzl, H. Kresse, and W. Weissflog, Liq. Cryst. **5**, 529 (2003); R. Stannarius, J. Li, and W. Weißflog, Phys. Rev. Lett. **90**, 025502 (2003).
[21] P. G. de Gennes, *The Physics of Liquid Crystals* (Clarendon Press, Oxford, 1979).
[22] See EPAPS Document No.E-PLEEE8–74–R22608 for a video of the experiment of Fig. 3. For more information on EPAPS, see http://www.aip.org/pubservs/epaps.html